Observed heterogeneities after hydration of MX-80 bentonite under pellet/powder form

Fabien Bernachy-Barbe, Nathalie Conil, William Guillot, Jean Talandier

Observed heterogeneities after hydration of MX-80 bentonite under pellet/powder form

Fabien Bernachy-Barbe[1]*, Nathalie Conil[2], William Guillot[1], Jean Talandier[3]

[1]Den-Service d'Etude du Comportement des Radionucléides (SECR), CEA, Université Paris-Saclay, F-91191, Gif-sur-Yvette, France.

[2]Andra, R&D Division, Meuse/Haute-Marne Underground Research Laboratory, 55290 Bure, France.

[3]Andra, R&D Division, 1-7 Rue Jean Monnet, F-92298 Chatenay Malabry, France.

*(corresponding author - email: fabien.bernachy-barbe@cea.fr)

Abstract

Bentonite is considered for engineered barriers in radioactive waste geological repositories due to its low permeability, swelling pressure and radionuclide retention properties. The French concept favors the use of bentonite under granular form - pellets and crushed pellets mix - for an easier building of plugs and seals relatively to bricks. However, this introduces a significant degree of macroscopic initial heterogeneity (at several scales) that is expected to disappear via mass redistribution during resaturation in order to obtain homogeneous hydraulic and mechanical performance. This also may have practical effects on the reliability of results from tests with small volumes of bentonite compatible with the time scales manageable at the laboratory. In this study, isochoric swelling pressure tests at various densities and sample sizes were carried out and evidenced bias mainly due to the size of the cell compared to the size of the pellets, although the average density is equivalent, pointing towards incomplete homogenization. Large-scale swelling pressure tests, however, converged towards values previously measured for more finely grained materials. Local pressure measurements also evidenced some stress heterogeneities that do not seem to disappear at medium time-scales. These stress heterogeneities could be correlated to local density variations of the final state assessed using destructive measurements and X-ray computed tomography.

Keywords

Bentonite, swelling pressure, heterogeneity, hydromechanical behavior

Article

1. Introduction

Preventing the release of radionuclides into the biosphere is the central issue of high- and intermediate-level nuclear waste geological repositories. The large swelling capacity, low permeability and radionuclide retention properties of bentonites make them desirable materials for building engineered barriers (plugs and seals) (Delage et al., 2010; Cui, 2017). Several bentonite-based materials (pure bentonite, bentonite-sand, etc.) are thoroughly studied in research programs of a number of countries. In the French CIGEO concept, pure MX-80 bentonite is proposed to build the seals in access galleries and shafts.

In order to facilitate the placement of large volumes of bentonite underground with a target density constraint, it is proposed to use bentonite as a granular form, such as compacted pellets/powder mix, thus avoiding the relatively complex building operations associated for instance with compacted bentonite bricks. The feasibility of implementing such a full-scale seal concept has been recently assessed in the framework of the European DOPAS project with the FSS experiment (Bosgiraud et al., 2015; Conil et al., 2015)(Figure 1). This large-scale mock-up allowed to investigate technologies required for the construction of a bentonite plug, as well as the density attained and properties of the remaining technological voids. This surface demonstrator made use of a 36 m long concrete structure mimicking an underground gallery of 7.6 m in diameter that was sealed with a bentonite core, between low-pH concrete containment plugs. No resaturation of the bentonite was attempted. The granular material used is composed of approximately 80% of 32 mm diameter pellets and 20% of crushed pellets in dry mass. Although the hydromechanical behavior of analogous granular materials has already been studied (Imbert and Villar, 2006; Hoffmann et al., 2007), the evaluation of the homogeneity of the final saturated state requires additional work. Indeed, the performance of such a structure can be dependent on the homogenization of the bentonite core at resaturation. Lower density regions could lead to higher hydraulic conductivity or reduced hydromechanical properties

that should not degrade the expected performance of these structures (Nasir et al., 2017). The resulting heterogeneities in the hydraulic properties of such a structure may be due to (Figure 1):

1. Large gaps and technological voids – decimeter to meter scale – (Mokni et al., 2016) in top areas due to incomplete filling, or large scale density gradients due to possible segregation of pellets for example; issues mitigated by a careful filling process,
2. Local density variations – millimeter to centimeter scale – (pellet/powder/macroporosity), that are expected to resorb through resaturation, as evidenced for example through X-ray microtomography (Van Geet et al., 2005),
3. Interface effects, which may have different hydraulic properties than the bulk due to thermal or, in the present case, chemical alteration, in particular with concrete structures (Herbert et al., 2004, 2008; Sanchez et al., 2006; Yamaguchi et al., 2007; Marty et al., 2010; Fernandez et al., 2017), that could be mitigated by the choice (if possible) of compatible materials.

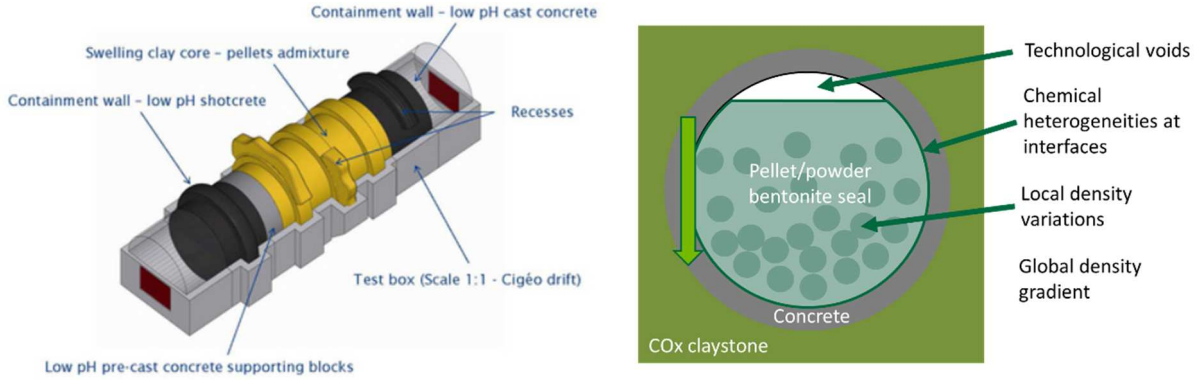

Figure 1: The DOPAS-FSS demonstrator (Bosgiraud et al., 2015) and sources of heterogeneities of a bentonite plug.

In this paper, laboratory characterizations of the pellet-powder bentonite material designed for the DOPAS-FSS demonstrator are presented. The objective is to investigate in representative conditions (constant volume, controlled water compositions, and targeted density values) the residual small scale heterogeneities (2. in the list above) in a resaturated granular bentonite material. These

heterogeneities are investigated through the effect of sample size on the swelling pressure kinetics and reached values, culminating with a currently ongoing metric scale experiment (called “REM”) implemented in the framework of the DOPAS project (Conil et al., 2015). Local total pressures and local density were also evaluated for an intermediate scale test.

2. Materials and methods

2.1. Studied material

The studied pellet/powder MX-80 bentonite is similar but with pellets of larger dimensions to what has been studied in (Molinero Guerra et al., 2017, 2018b). It is composed in proportions of dry mass between 70%/30% and 80%/20% of respectively ϕ 32 mm compacted pellets (Laviosa-MPC Expangel SP32) and crushed pellets (from the used pellets, Laviosa-MPC). The dry density of individual pellets was measured on average at 2.00 g/cm^3 using hydrostatic weighting in paraffine wax. Crushed pellets result in an apparent dry density of 1.249 g/cm^3 at placement in cells using only gravity and manual compaction. These materials were stored in air-tight containers at laboratory temperatures and tested at a controlled temperature of 22°C +/- 1°C. The initial water content of these materials was characterized one day before testing using a standard oven drying at 105°C for 24h procedure. This material is designated “FSS material” in the following.

The water composition used for most experiments was synthetic water similar to site water extracted at Andra’s underground laboratory (LSMHM – Laboratoire Souterrain de Meuse/Haute-Marne, Bure, France) with slightly lower salinity and the addition of a low AgCl concentration as an antimicrobial agent. Its formulation is presented in Table 1. Its pH was measured at 7.77 initially and unchanged after an exposure of 7 months at the atmosphere in the resaturation apparatus.

Salt	$NaHCO_3$	Na_2SO_4	NaCl	KCl	$CaCl_2$, $2H_2O$	$MgCl_2$, $6H_2O$	AgCl

Mass per litre of solution (g)	0.281	0.426	0.615	0.077	1.082	1.356	0.0001

Table 1: Synthetic site water elementary composition.

2.2. Experimental setups and plan

The basic operation of constant volume cells with axial hydration used at CEA is described in (Imbert and Villar, 2006) and not fully recalled here (Figure 2). These oedometric cells are equipped with axial force and displacement measurement, and hydration is carried out through the bottom of the samples with an injection pressure of 6.5 to 7.5 kPa. The injected water mass is measured continuously. Three different cell diameters were used (57 mm, 120 mm and 240 mm) and pellet powder mixes tested at various dry densities mostly around 1.5 g/cm^3. The properties of these samples are presented in Table 2. The largest cell (of diameter 240 mm) is equipped with radial pressure and relative humidity sensors. Cells are filled with bentonite by depositing pellets layer by layer and adding the powder to level the surface. This procedure aims at minimizing macroscopic voids at the top of the sample and having evenly distributed mass throughout the sample.

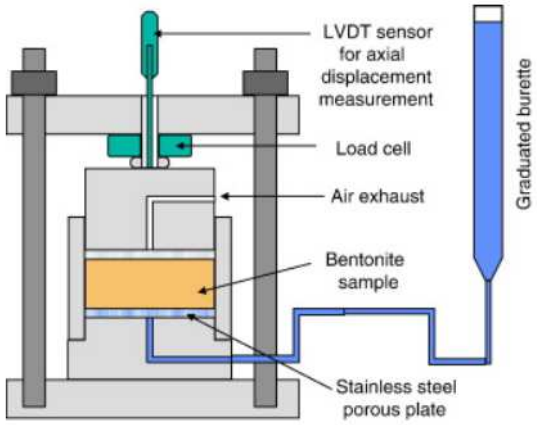

Figure 2: General principle of the oedometric cells used, extracted from (Imbert and Villar, 2006).

Reference	Diameter (mm)	Height (mm)	Initial water content (%)	Final dry density (g/cm^3)	Final swelling pressure (MPa)	Remarks
57_1	57	32.8	4.44	1.509	5.04	-
57_2	57	57.0	4.44	1.517	4.92	-
120_1	120	64.1	4.54	1.204	0.50	-
120_2	120	62.9	4.55	1.306	1.05	-
120_3	120	64.5	4.43	1.586	6.88	-
120_4	120	63.6	4.38	1.411	2.01	K=2.03.10^{-13} m/s
120_5	120	64.2	4.36	1.493	3.51	K=1.21.10^{-13} m/s
120_6	120	64.2	4.40	1.544	4.82	K=9.66.10^{-14} m/s
120_7	120	67.3	4.24	1.511	4.54	-
240_1	240	65.6	4.23	1.451	2.39	-
240_2	240	67.2	4.42	1.475	2.39	-
240_3	240	105.4	4.23	1.516	3.84	With radial sensors, dismantled

Table 2: Summary of isochoric swelling pressure tests carried out.

3. Experimental results

3.1. Effect of the sample size on the swelling pressure and heterogeneities

3.1.1.Laboratory scale tests

The dry density - swelling pressure relationship for a constant sample size follows a power or exponential law in a classical way similar to published results (Dixon et al., 1996; Karnland et al., 2008; Villar et al., 2012; Cui, 2017). The swelling kinetics exhibit (Figure 3) two to three inflection points, characteristic of the collapse of the macropores or voids between the pellets (Alonso et al., 2011; Gens et al., 2011). After saturation, the hydraulic conductivity was measured on the samples 120_4, 120_5,

and 120_6 under a 6 bar pressure difference (Table 2). The hydraulic conductivity was obtained from the average of in and out water volumes recorded for a minimum of 50 days after equalization of the input and output flows.

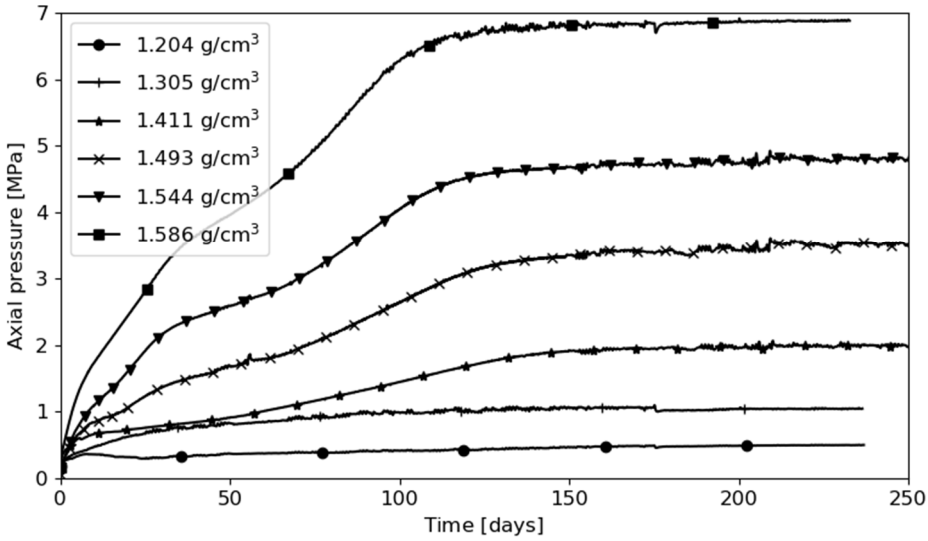

Figure 3: Swelling pressure kinetics measured through axial pressure in diameter 120 mm oedometric cells, for six final dry densities of the FSS material (tests 120_1 to 120_6).

It is observed that all parameters held constant, times to saturation approximately scale with the square of sample height (Figure 4), as is classically observed, but the final obtained swelling pressure appears to be independent of this parameter. However, it is observed that asymptotic swelling pressure values do not depend uniquely on the average dry density but also exhibit a consistent size dependency relatively to the sample diameter: a 24% decrease from 5 MPa to 3.8 MPa is recorded when going from diameter 57 mm (with one pellet) to 240 mm (with three pellet layers). This may be possibly attributed to a lack of representativeness of the studied sample due to a predominant wall effect in the case of small samples, or friction issues. In each of these cases, such size dependency should be associated with a heterogeneity of the sample stress field.

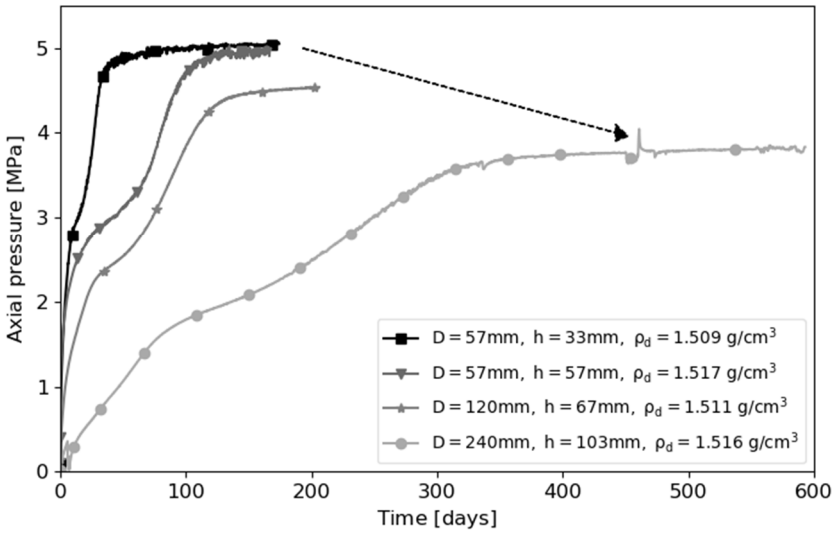

Figure 4: Decreasing trend in swelling pressure curves for four sample geometries (tested at approximately 1.51 g/cm^3 dry density: the legend indicates cell diameter (d), sample height (h) and final dry density (tests 57_1, 57_2, 120_7 and 240_3).

The results are compared in Figure 5 with a material with a much smaller heterogeneity length scale (similar to the one described in (Molinero Guerra et al., 2017)) and composed of 7 mm MX-80 pellets (Laviosa-MPC Expangel SP7) and powder, previously characterized at CEA (Gatabin et al., 2016). This material is designated as “PGZ material” in the following. It has been studied using the same devices with samples approximately 76 cm^3 in volume (57 mm in diameter and around 30 mm in height). The pellet to sample diameter ratio (d/D) is therefore similar to the largest test carried out with the FSS material (PGZ: d/D=7/57=0.12, FSS: d/D=32/240=0.13). It can be observed that the final swelling pressure for the FSS material converges with increasing sample sizes towards the final swelling pressure for the “finer” PGZ material.

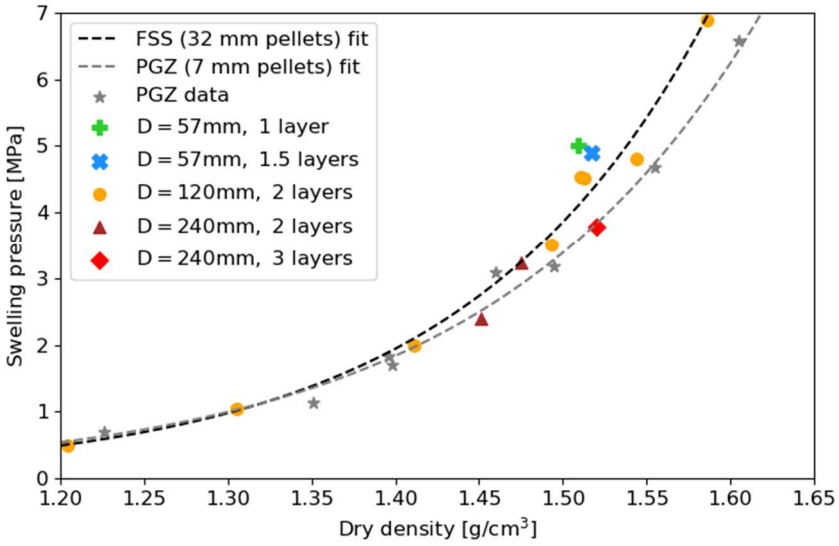

144

145 Figure 5: Swelling pressure vs. final sample dry density for MX-80 based materials determined with

146 samples of various sizes, and exponential fits.

147 Such data may point to the existence of a representative volume size that could be defined relative to

148 the pellet size. The size effect observed here should be linked to residual heterogeneities in density,

149 and therefore in swelling pressure, that do not appear to be eliminated at least at “short” timescales

150 (accessible at the lab). The exponential fits on the FSS and PGZ data seem to qualitatively indicate that

151 behaviors are increasingly different as a function of the average dry density. This could point at easier

152 mass and stress redistribution for lower average dry densities (due to the different hydromechanical

153 behavior and/or lower friction) and therefore a weaker size dependency of the results.

154 3.1.2.Local pressure measurements of test 240_3

155 Remaining heterogeneities are more easily demonstrated through direct measurements. For this

156 reason, the large volume test (diameter 240 mm, height 103 mm) is instrumented with radial pressure

157 measurements (with membrane diameter 7 mm) and relative humidity sensors plunging into the

158 bentonite core (Figure 6 and Table 3). The test was conducted for 1214 days and reached 3.84 MPa

159 average axial swelling pressure with near-constant sensor values between 600 days and dismantling;

160 hence only the first 600 days are represented in the following figures. The injected water mass shows

161 a constant increase between 600 days and dismantling at a rate of approximately 110 mg/day (not
162 shown) although that could be attributed to incomplete saturation of the upper regions of the
163 specimen or other instrumental reasons (evaporation of the water reserve, drifts of the measurement
164 apparatus).

165 The relative humidity sensors (Figure 7, top) show a response characteristic of 1D wetting; starting
166 initially at 28%, the sensor closest to the hydration surface reaches 100% at approximately 19 days.
167 This sensor at elevation 20 mm from the surface shows must faster kinetics than the sensor at 40 mm
168 elevation whose (large) pores are fully saturated at 200 days: this points towards a fast intrusion of
169 liquid water into the large pores in the first centimeters of the sample, forming quickly a low
170 permeability plug. Some sensors still show values below 100% RH at 300 days of hydration.

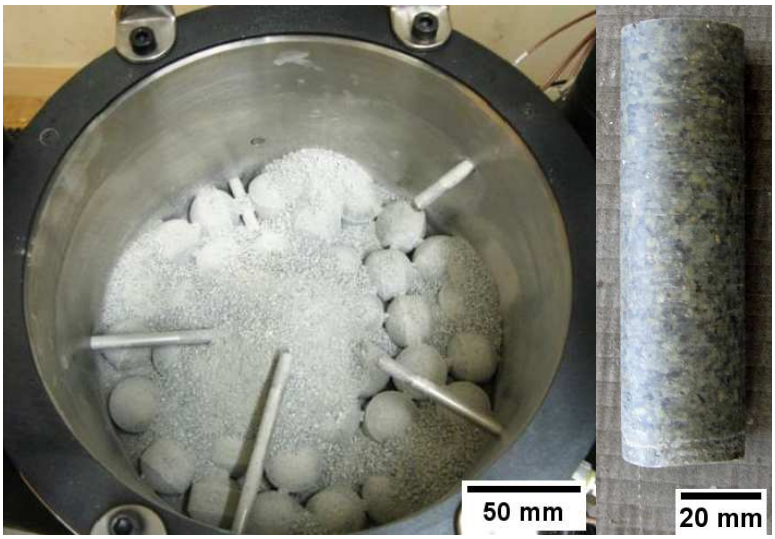

171

172 Figure 6: Photograph of the ϕ240 mm cell being filled with 32 mm pellets and crushed pellets, with
173 RH sensors visible (left) and ϕ30 mm core obtained at dismantling, showing no visible trace of the
174 pellets (right).

Z (mm)	Designation	Θ (°)	r (mm)	Final value
20	HR1	0	40	-
	P1	0	0	**4.43 MPa**

40	HR2	72	70	(100%)
	P2	90	0	-
60	HR3	144	100	(100%)
	P3	180	0	**3.74 MPa**
80	HR4	216	70	(100%)
	P4	270	0	**4.69 MPa**
100	HR5	288	40	(100%)

175

176 Table 3: Summary of the positions of radial sensors (P for total pressure and HR for relative humidity)
177 in the 240 mm cell: *Z* (axial elevation from the bottom hydration surface), *Θ* (angular position) and *r*
178 (radial position measured from the cell surface).

179 Local radial pressure measurements (Figure 7, bottom) show kinetics qualitatively similar to the
180 average axial swelling pressure, although delayed as a function of their position relative to the
181 hydration front. Regarding asymptotic values, no conclusions can be drawn relative to the vertical
182 positions, indicating that local pressure values are influenced mostly by the local density at placement
183 (a pellet in front of the sensor could explain large values). The axial swelling pressure seems to be
184 mostly lower than the radial pressures in agreement with another paper (Molinero Guerra et al.,
185 2018b), which may be due to the lower average dry density at placement at the upper surface.
186 However, the total sensor surface is probably insufficient to confirm swelling anisotropy (Cui, 2017).
187 Moreover, these radial pressure heterogeneities (of order 1 MPa) do not disappear at the studied time
188 scales (1214 days) through some relaxation mechanism.

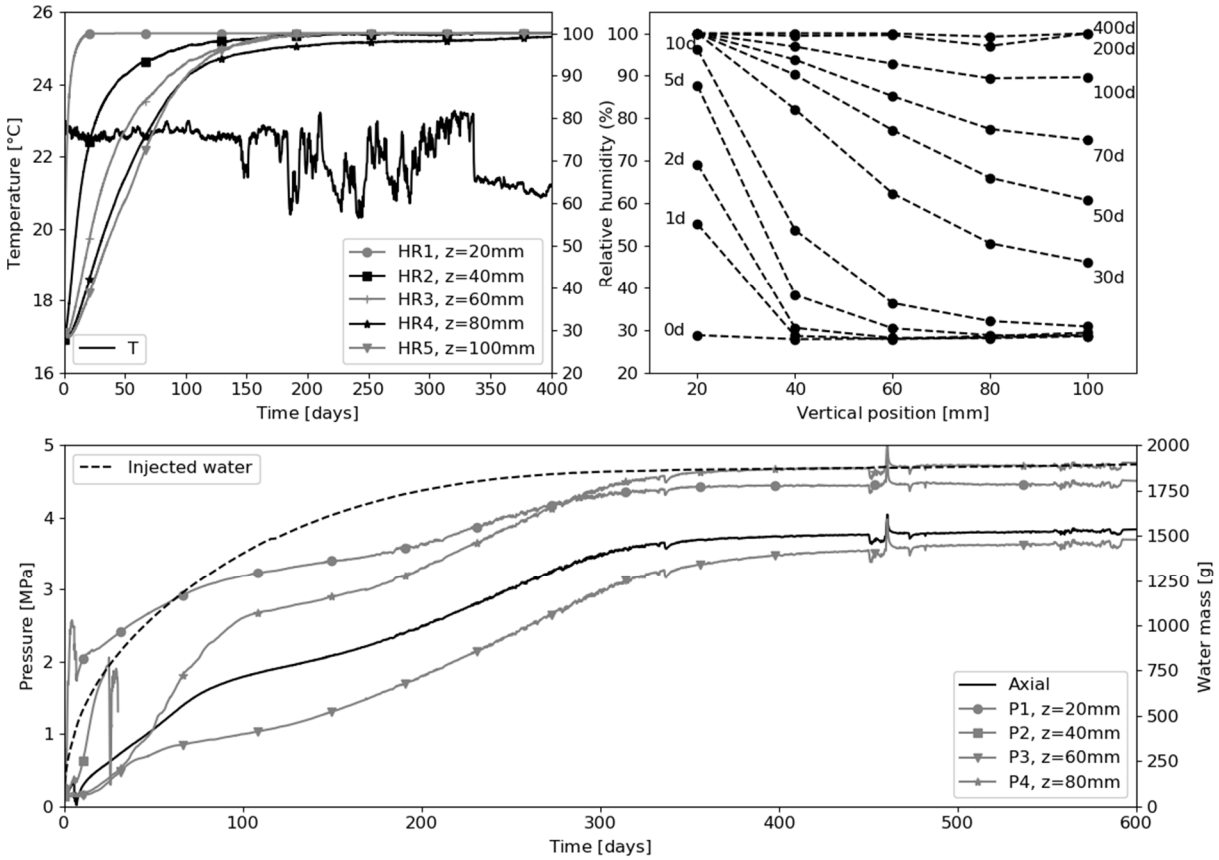

Figure 7: Relative humidity and temperature evolution measured in the 240 mm test (top left), resulting in relative humidity profiles (top right) and total pressure measurements with the total injected water mass (bottom). Sensor P2 stopped functioning early.

3.1.3. Dismantling and local measurements on sample 240_3

The 240 mm diameter test was dismantled in order to evaluate the density and water content heterogeneities of the final state of the material, coring was performed directly in the cell using a ϕ 30 mm cutting tool designed to avoid mechanical or friction heat damage of the sample without any cooling or lubrication. The top part of the sample is however exposed to air when extracting cores (timescale of approximately 1 hour) and superficial drying is unavoidable, inducing small cracks in the top side of the cores.

Six cores were obtained at various locations of the bentonite core (in front of pressure sensors, in the center, and at one random mid-radius position) and each was split into two same-sized samples at four

vertical positions. Water content was measured using 105°C oven drying for 24h and the apparent density from hydrostatic weighing in oil. The locally measured water content is used to compute the local dry density; the average profiles are provided in Figure 8. It was first checked that the average properties correspond to the expected value (measured dry density of 1.517 g/cm^3 for an expected value of 1.516 g/cm^3 using initial material data and measured water content of 29.16% for an expected value of 29.97%, also pointing towards slightly incomplete saturation). A dry density gradient of approximately 2.4% is observed between the averages of the lowest and highest samples, and density is approximately constant between the samples at elevation 65 mm and 90 mm.

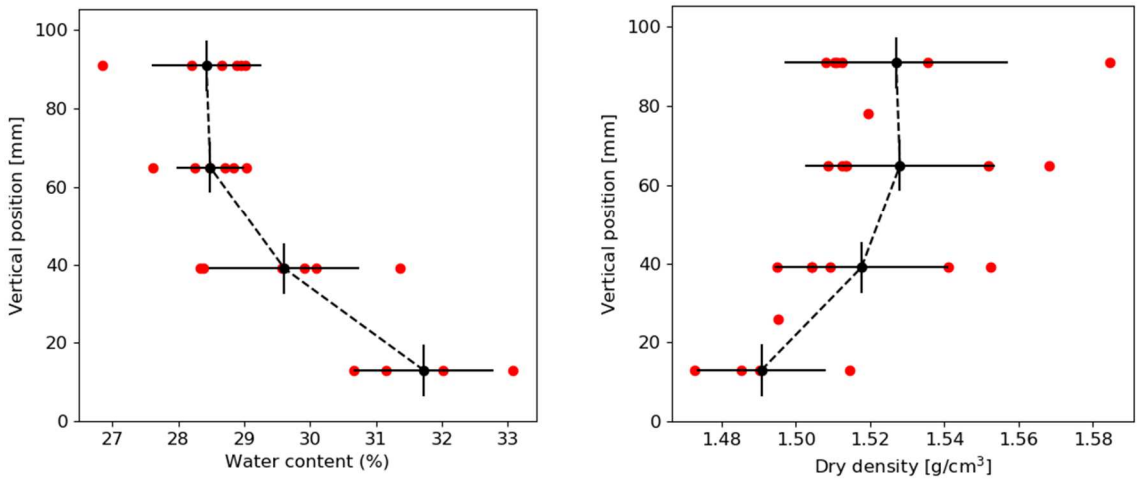

Figure 8: Water content and dry density vertical profiles measured at dismantling of test 240_3, with mean and standard deviations. Considering the difficult sample slicing, an error bar corresponding to half the thickness of samples is introduced in the vertical position.

Four cores were conditioned into vacuum-sealed aluminum bags and imaged using X-ray Computed Tomography (X-CT) using a GE phoenix v|tome|x m instrument (tube parameters 200 kV/180 µA using 2200 projections composed of 3 averaged images). In order to detect small density variations at a large scale, the average gray levels over 5 vertical slices were computed (Figure 9): a vertical gradient of X-ray absorption of approximately 2-3% is observed in a consistent way with hydrostatic weighing measurements. Some moderate discrepancy is observed in the top part of the specimen, assumed to

be due to the incomplete filling of the microcracks at the top of the sample; resulting in an overestimation of the apparent volume. Assuming homogeneous elementary composition (and specific attenuation coefficient), density variations of order 1% can be seen with a characteristic size compatible with the pellet size (ϕ 32mm), pointing to small but detectable density heterogeneities. Considering the careful placement process, the global density gradient is inconsistent with initial heterogeneities and must be a result of the wetting and swelling process. A possible mechanism for this mass transport is an upwards transport of material into the macroporosity of the dryer regions as well as compaction induced by the initially swelling bottom regions, as observed from DVC (Digital Volume Correlation) in (Molinero Guerra et al., 2018a), although these authors did not attempt a detection of small density variations.

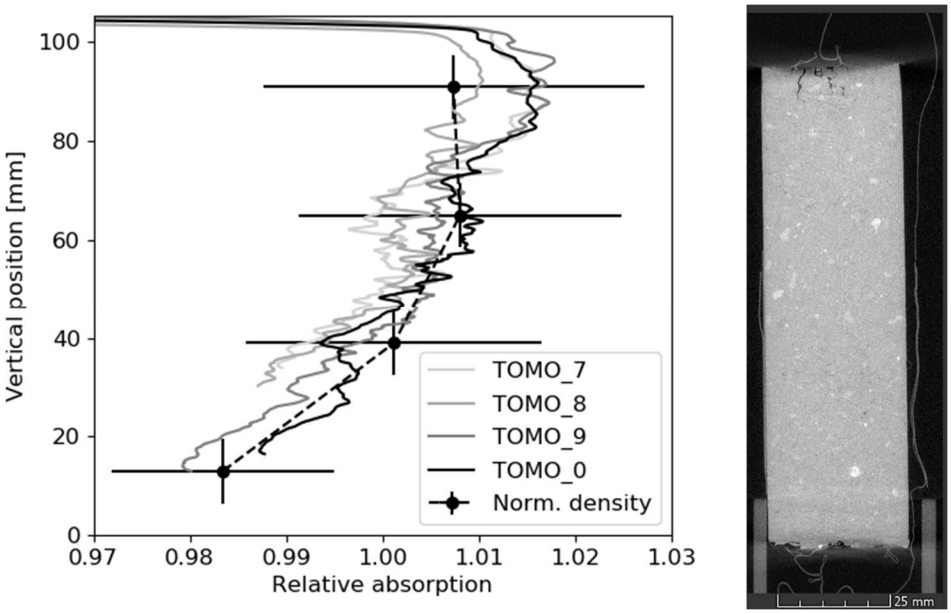

Figure 9: Vertical profiles of the normalized grey levels for four cores' CTs compared with the normalized density estimate (right) and example vertical slice of a bentonite core obtained with X-CT (left).

3.1.4.Towards full-scale seals: early analysis of the REM experiment

The REM (Resaturation à l'Échelle Métrique) experiment is part of a common program with the FSS construction experiment and will demonstrate the resaturation of the bentonite pellet/powder

mixture used in FSS and analyze the mixture behavior during resaturation at a metric scale unachievable with standard laboratory cells. The three objectives are the following:

1. To change the scale from the lab tests which defined the used mixture of pellets and crushed bentonite. This test must be carried out at a metric scale at least in order to be representative of the FSS experiment;
2. To demonstrate the resaturation of the bentonite mixture at this scale and to study the phenomenology and kinetics involved in achieving saturation;
3. To check that the hydraulic behavior involved in achieving saturation is generally uniform at this scale. Once fully saturated, to check that the hydraulic characteristics (gas entry pressure, water and gas permeability) and mechanical characteristics (swelling pressure) are compliant with sealing specifications and are uniform at this scale.

In order to get as close as possible to in-situ conditions, several criteria were defined for the design. Although the pellet-powder admixture emplacement should be representative of the technique used in FSS (use of screw-type conveyors to transport materials), in particular the compacting rates, the reduced dimensions of REM prevent the use of the filling tool used in FSS. To ensure comparable properties (permeability, swelling pressure) between the REM model and the FSS demonstrator, the average dry density was made similar in both experiments. The dry density primarily depends on the compacting rate, residual void level, and initial water content.

The cell is cylindrical with a 1 m internal diameter and an inside height of 1 m. In order to facilitate filling and avoid “technological voids”, sensors were spread out with intervals of at least the size of the pellets. The vessel is a 40 mm thick cylinder, with two lids fitted with sintered stainless steel plates in the bottom part and air vents in the top part (Figure 10). The lids are fitted with an O-ring to ensure leak-tightness and are held onto the cylinder by four high-strength steel rods 72 mm in diameter. Two frames arranged in a square formation on each surface hold the load. All surfaces in contact with the bentonite and hydration water are made of stainless steel. The injection system supplies water to the

sample inside the surface and regulates and/or quantifies the volume of water provided. The output circuit collects air ejected from the vessel (Figure 10). A precise flowmeter measures the flowrate and a Relative Humidity (RH) measurement sensor is placed on a branch of the circuit.

The average dry density at the end of the filling process was measured at 1.510 g/cm^3 and the materials used had a water content of 5.0%. The hydration water is taken from a borehole located in the COX formation in the Andra URL at Bure (Vinsot et al., 2008). In practice, in-situ water flows are low (host rock permeability of the order of 10^{-13} m/s) and will not, therefore, modify the structure of the pellet/powder mixture by carrying away the smallest particles (erosion phenomena). The hydration rate was set at 50 ml per day, corresponding to in-situ measurements in Bure URL boreholes PAC1002 and POX1201 (Vinsot et al., 2011).

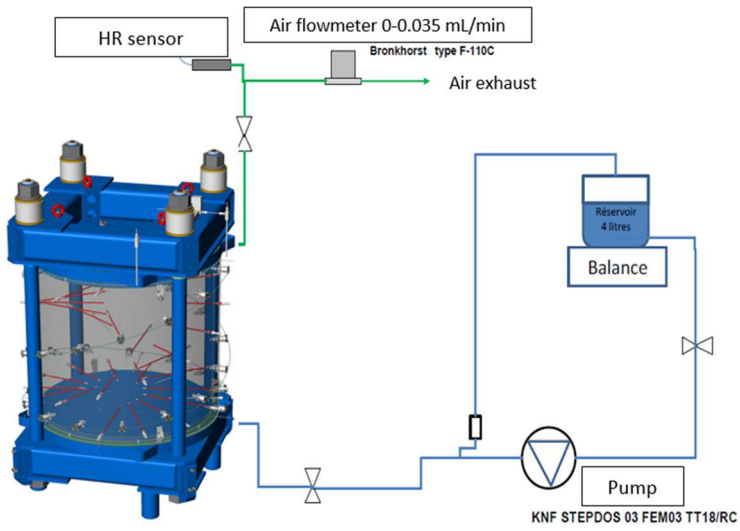

Figure 10: Schematic circuit diagram of the REM vessel and its environment.

The permeability of the bentonite mixture at target saturation in the FSS experiment must be lower than 10^{-11} m/s and therefore the duration of saturation for a metric-scale sample is very long (calculations estimate the saturation time at approximately 10 to 30 years and correlations with the lab-scale tests give results as high as 60 years). The sensors must be sufficiently unobtrusive to measure

the inside surface as closely as possible and sufficiently robust to function for as long as possible. Five different types of measurements are carried out: total radial and axial pressure, pore pressure, relative humidity, and temperature. The radial sensors are distributed at various heights in a spiral around the cell, perpendicular to the hydration flow (Figure 11).

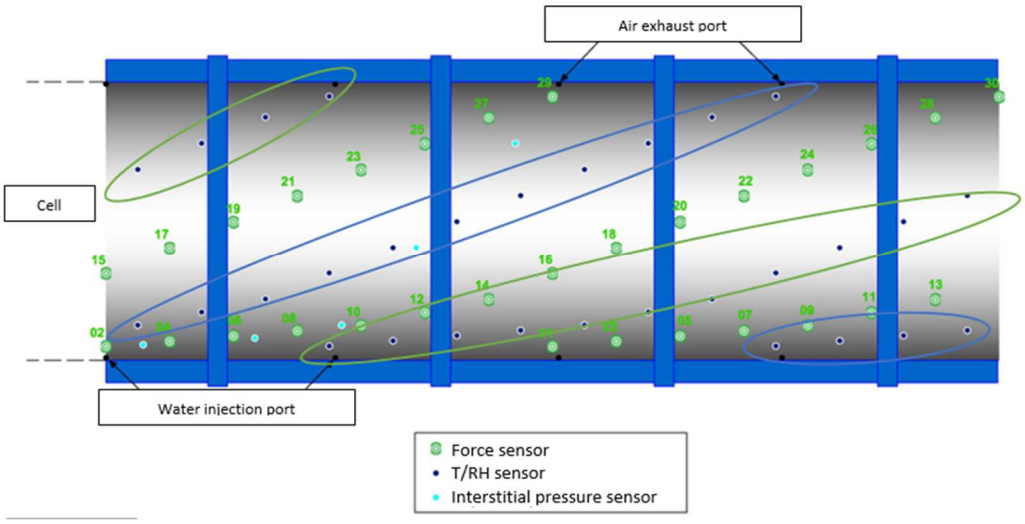

Figure 11: Schematic of the cell "unwrapped" showing sensors on the REM experiment vessel, (left) (section 1 in green, section 2 in blue) and photography of the experiment currently running (right).

Thirty humidity/temperature sensors were installed in the vessel. A diagram showing the sensor locations is given in Figure 11. Relative humidity measurements are presented in Figure 12. To facilitate comprehension of the results, measurements are broken down by section (Figure 11), with 20 mm spacing between each sensor of a section from HUM_01 to HUM_10, and then a constant spacing of 100 mm. RH was at about 27% at the start of hydration. The most reactive sensors were sensors 01/03/05 in section 1 that reached 100% due to their proximity to the injection system. A first response is detected at 700 mm of the hydration front (sensors 23 & 24), after 1600 days. It can be observed that three sensors have a different response with increasing and decreasing phases. In light of these results, it is clear that the homogenization process will probably be long, as suggested by the estimations (60 years to reach total saturation). As expected by the low RH levels there is almost no response of the total pressure sensors (at noise levels, +/- 0.03 MPa) at any point of the cell.

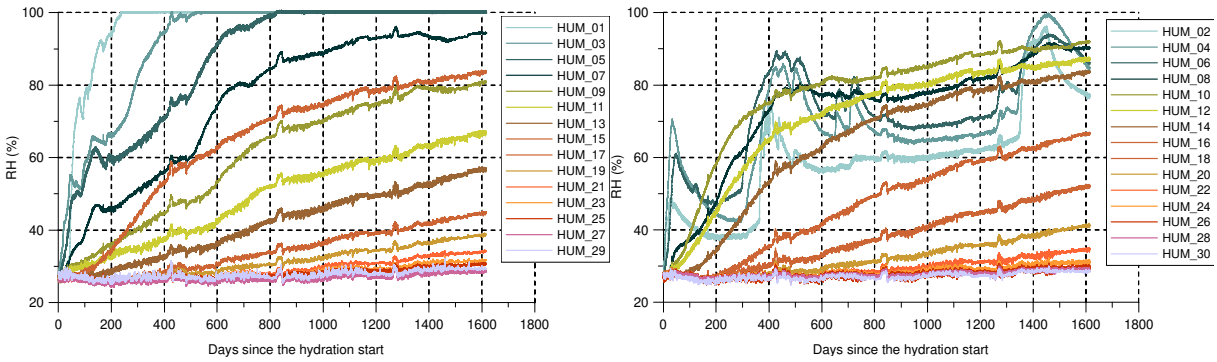

Figure 12: Present state of the experiment: relative humidity sensors for the two sections ordered from the bottom (1&2) to top (29&30).

4. Conclusions

The homogenization of bentonite seals upon resaturation in engineered barriers is a desirable property to justify their hydromechanical performance. The swelling behavior upon infiltration of pellet/powder samples of different sizes and densities was therefore studied in constant volume cells. A dependence of the swelling pressure on the diameter of samples was observed, possibly caused by friction effects or lack of representativeness for a large pellet-to-sample size ratio. Measurements showed large local stress heterogeneities that do not disappear upon saturation, that can be only explained by the local environment of the sensor and small residual density variations. Local density variations coming from the pellet/powder structure are indeed detected in a long-term experiment. Finally, the existence of a significant density gradient in the direction of hydration was demonstrated, that can be caused only by the hydration and swelling process itself. Therefore, a metric scale bentonite resaturation experiment “REM” was designed and its initial four-year results are presented, with at this stage no measured swelling pressure. Its measurements over the next decades are expected to provide insights on the behavior of bentonite pellet/powder plugs at a scale relevant for the geological repositories.

Acknowledgements

This work was supported by Andra in the framework of the CEA/Andra agreement.

References

317 Alonso, E.E., Romero, E., Hoffmann, C., 2011. Hydromechanical behaviour of compacted granular
318 expansive mixtures: experimental and constitutive study. Geotechnique 61, 329–344.
319 Bosgiraud, J.M., Bourbon, X., Pineau, F., Foin, R., 2015. The DOPAS full scale seal experiment (FSS): An
320 industrial prototype for Cigeo. Presented at the NUWCEM 2014.
321 Conil, N., Talandier, J., Noiret, A., Armand, G., Bosgiraud, J.M., 2015. Report on Bentonite Saturation
322 Test (REM) (DOPAS WP4 Deliverable No. D4.2).
323 Cui, Y.-J., 2017. On the hydro-mechanical behaviour of MX80 bentonite-based materials. J. Rock
324 Mech. Geotech. Eng. 9, 565–574. https://doi.org/10.1016/j.jrmge.2016.09.003
325 Delage, P., Cui, Y.J., Tang, A.M., 2010. Clays in radioactive waste disposal. J. Rock Mech. Geotech.
326 Eng. 2, 111–123. https://doi.org/10.3724/SP.J.1235.2010.00111
327 Dixon, D.A., Gray, M.N., Graham, J., 1996. Swelling and hydraulic properties of bentonites from
328 Japan, Canada and USA. Proc. 2nd Int. Congr. Environ. Geotech. 1, 43–48.
329 Fernandez, R., Torres, E., Ruiz, A.I., Cuevas, J., Cruz Alonso, M., Garcia Calvo, J.L., Rodriguez, E., Jesus
330 Turrero, M., 2017. Interaction processes at the concrete-bentonite interface after 13 years of
331 FEBEX-Plug operation. Part II: Bentonite contact. Phys. Chem. Earth 99, 49–63.
332 https://doi.org/10.1016/j.pce.2017.01.009
333 Gatabin, C., Guillot, W., Touzé, G., Bernachy, F., 2016. Etude des transferts de gaz dans la bentonite -
334 Scellements en forages de petits diamètres - Expérimentation PGZ 1022 (Note Technique).
335 CEA.
336 Gens, A., Valleján, B., Sánchez, M., Imbert, C., Villar, M. v., Van Geet, M., 2011. Hydromechanical
337 behaviour of a heterogeneous compacted soil: experimental observations and modelling.
338 Géotechnique 61, 367–386. https://doi.org/10.1680/geot.SIP11.P.015
339 Herbert, H.-J., Kasbohm, J., Moog, H.C., Henning, K.-H., 2004. Long-term behaviour of the Wyoming
340 bentonite MX-80 in high saline solutions. Appl. Clay Sci., Clays in Natural and Engineered
341 Barriers for Radioactive Waste Confinement 26, 275–291.
342 https://doi.org/10.1016/j.clay.2003.12.028
343 Herbert, H.-J., Kasbohm, J., Sprenger, H., Fernández, A.M., Reichelt, C., 2008. Swelling pressures of
344 MX-80 bentonite in solutions of different ionic strength. Phys. Chem. Earth Parts ABC, Clays
345 in Natural & Engineered Barriers for Radioactive Waste Confinement 33, S327–S342.
346 https://doi.org/10.1016/j.pce.2008.10.005
347 Hoffmann, C., Alonso, E.E., Romero, E., 2007. Hydro-mechanical behaviour of bentonite pellet
348 mixtures. Phys. Chem. Earth Parts ABC, Clay in natural and engineered barriers for
349 radioactive waste confinement - Part 2 32, 832–849.
350 https://doi.org/10.1016/j.pce.2006.04.037
351 Imbert, C., Villar, M.V., 2006. Hydro-mechanical response of a bentonite pellets/powder mixture
352 upon infiltration. Appl. Clay Sci. 32, 197–209. https://doi.org/10.1016/j.clay.2006.01.005
353 Karnland, O., Nilsson, U., Weber, H., Wersin, P., 2008. Sealing ability of Wyoming bentonite pellets
354 foreseen as buffer material – Laboratory results. Phys. Chem. Earth Parts ABC, Clays in
355 Natural & Engineered Barriers for Radioactive Waste Confinement 33, S472–S475.
356 https://doi.org/10.1016/j.pce.2008.10.024
357 Marty, N.C.M., Fritz, B., Clement, A., Michau, N., 2010. Modelling the long term alteration of the
358 engineered bentonite barrier in an underground radioactive waste repository. Appl. Clay Sci.
359 47, 82–90. https://doi.org/10.1016/j.clay.2008.10.002
360 Mokni, N., Barnichon, J.-D., Dick, P., Nguyen, T.S., 2016. Effect of technological macro voids on the
361 performance of compacted bentonite/sand seals for deep geological repositories. Int. J. Rock
362 Mech. Min. Sci. 88, 87–97. https://doi.org/10.1016/j.ijrmms.2016.07.011
363 Molinero Guerra, A., Aimedieu, P., Bornert, M., Cui, Y.-J., Tang, A.M., Sun, Z., Mokni, N., Delage, P.,
364 Bernier, F., 2018a. Analysis of the structural changes of a pellet/powder bentonite mixture
365 upon wetting by X-ray computed microtomography. Appl. Clay Sci. 165, 164–169.
366 https://doi.org/10.1016/j.clay.2018.07.043
367 Molinero Guerra, A., Cui, Y.-J., Mokni, N., Delage, P., Bornert, M., Aimedieu, P., Tang, A.M., Bernier,
368 F., 2018b. Investigation of the hydro-mechanical behaviour of a pellet/powder MX80

bentonite mixture using an infiltration column. Eng. Geol. 243, 18–25. https://doi.org/10.1016/j.enggeo.2018.06.006
Molinero Guerra, A., Mokni, N., Delage, P., Cui, Y.-J., Tang, A.M., Aimedieu, P., Bernier, F., Bornert, M., 2017. In-depth characterisation of a mixture composed of powder/pellets MX80 bentonite. Appl. Clay Sci. 135, 538–546. https://doi.org/10.1016/j.clay.2016.10.030
Nasir, O., Nguyen, T.S., Barnichon, J.D., Millard, A., 2017. Simulation of hydromechanical behaviour of bentonite seals for containment of radioactive wastes. Can. Geotech. J. 54, 1055–1070. https://doi.org/10.1139/cgj-2016-0102
Sanchez, L., Cuevas, J., Ramirez, S., Riuiz De Leon, D., Fernandez, R., Vigil Dela Villa, R., Leguey, S., 2006. Reaction kinetics of FEBEX bentonite in hyperalkaline conditions resembling the cement-bentonite interface. Appl. Clay Sci. 33, 125–141. https://doi.org/10.1016/j.clay.2006.04.008
Van Geet, M., Volckaert, G., Roels, S., 2005. The use of microfocus X-ray computed tomography in characterising the hydration of a clay pellet/powder mixture. Appl. Clay Sci. 29, 73–87. https://doi.org/10.1016/j.clay.2004.12.007
Villar, M.V., Gómez-Espina, R., Gutiérrez-Nebot, L., 2012. Basal spacings of smectite in compacted bentonite. Appl. Clay Sci. 65–66, 95–105. https://doi.org/10.1016/j.clay.2012.05.010
Vinsot, A., Delay, J., de La Vaissière, R., Cruchaudet, M., 2011. Pumping tests in a low permeability rock: Results and interpretation of a four-year long monitoring of water production flow rates in the Callovo-Oxfordian argillaceous rock. Phys. Chem. Earth Parts ABC, Clays in Natural & Engineered Barriers for Radioactive Waste Confinement 36, 1679–1687. https://doi.org/10.1016/j.pce.2011.07.091
Vinsot, A., Mettler, S., Wechner, S., 2008. In situ characterization of the Callovo-Oxfordian pore water composition. Phys. Chem. Earth Parts ABC, Clays in Natural & Engineered Barriers for Radioactive Waste Confinement 33, S75–S86. https://doi.org/10.1016/j.pce.2008.10.048
Yamaguchi, T., Sakamoto, Y., Akai, M., Takazawa, M., Iida, Y., Tanaka, T., Nakayama, S., 2007. Experimental and modeling study on long-term alteration of compacted bentonite with alkaline groundwater. Phys. Chem. Earth 32, 298–310. https://doi.org/10.1016/j.pce.2005.10.003